Entropy production and energy dissipation in symmetric redox supercapacitors

N. Palma-Aramburu and I. Santamaría-Holek
UMDI-Facultad de Ciencias, Universidad Nacional Autónoma de México, Campus Juriquilla, Boulevard Juriquilla 3001, Juriquilla 76230, Querétaro, Mexico
(Received 10 May 2017; published 2 August 2017)

In this work we propose a theoretical model that accounts for the main features of the loading-unloading process of a symmetric redox MnO_2-based supercapacitor dominated by fast electrochemical reactions at the electrodes. The model is formulated on the basis of nonequilibrium thermodynamics from which we are able to deduce generalized expressions for the electrochemical affinity, the load-voltage and the current-voltage equations that constitute generalizations of the current-overpotential and Butler-Volmer equations, and that are used to describe experimental voltagram data with good agreement. These equations allowed us to derive the behavior of the energy dissipated per cycle showing that it has a nonmonotonic behavior and that in the operation regime it follows a power-law behavior as a function of the frequency. The existence of a maximum for the energy dissipated as a function of the frequency suggests the that the corresponding optimal operation frequency should be similar in value to $\omega_{\max}$.

DOI: 10.1103/PhysRevE.96.022103

I. INTRODUCTION

The current energy demand and the need of improvement of electrochemical storage devices has intensified both scientific and industrial research in order to increase their energy conversion, efficiency, and safeness, as well as to reduce their cost, size, and environmental impact. Among the most common and widely used electrochemical storage and energy conversion devices are batteries, fuel cells, and capacitors. In the last decades, many materials, synthesis techniques, and improved electrode morphologies have been proposed in order to increase both their storage capacity and their energy efficiency [1].

Recently electrochemical capacitors (ECs) or supercapacitors have received a lot of attention due to their high power density, high cycling stability, long shelf life, high efficiency, wide range of operating temperatures, and high energy conversion rates [2–5]. The EC systems still have several challenges to overcome, such as low-energy densities, high production cost, and low specific capacitance; this has promoted an intense research for electrode materials that have both high specific surface and porosity [6,7].

The EC can be categorized in two types: the first are the electrical double-layer supercapacitors, in which their capacitance is due to electrostatic charge accumulation in the electrode surface and there is no charge transfer or net ion exchange between the electrode and the electrolyte; and second, the faradaic supercapacitor, or pseudocapacitor, in which there is a charge transfer between the electrode and the electrolyte by means of a redox reaction, an intercalation process or an electrosorption on the surface of the electrode that changes the oxidation state through an external potential applied to the cell [8]. It is important to mention that faradaic and nonfaradaic processes may be simultaneously present in a supercapacitor, as the so-called hybrid capacitors, as the lithium-ion capacitor.

In this article we analyze a pseudocapacitor subject to redox reactions as the ones that happen in electrodes based in transitions metals, for example, RuO_2, MnO_2, and Co_3O_4 [9–11], in order to describe the hysteresis loop and the energy dissipation during rapid charging or discharging processes. We chose to study this type of electrode material because the chemical kinetics dominates the whole capacitor dynamics over ion transport phenomena. This includes the overcoming of the double layer potential, the ion diffusion in the electrolyte, in the surface and inside the nanoparticle, and the intercalation and insertion process among other effects.

We based our description on chemical kinetics as derived from Onsager's nonlinear irreversible thermodynamics [12,13]. It allows us to derive a Langevin equation that describes the charging or discharging process. This procedure is very rich since it allows us to replicate the hysteresis loop, to obtain a scaling law behavior for the dissipated energy in the low- and high-frequency regime and the entropy production per cycle. Even more important is the fact that the Onsager formalism is consistent with the Butler-Volmer equation, which has been generalized in other contexts in order to include nonidealities, for instance, phase transitions [14], hysteresis [15], electrodeposition [16], electrocatalysis [17], Li-ion insertion batteries [18,19], concentrated solutions [20], adsorption [21], double layer effects [22,23], and nonequilibrium [20,24], among others.

Hysteresis emergence translates into several technical difficulties and limits possible industrial applications; it is present in many areas ranging from physical phenomena (such as ferromagnetic, ferroelectric, and elastic materials), chemical reactions, and weather dynamics to social and economic sciences. Systems in which the enclosed area of the hysteresis loop depends on the frequency of the input variable are called rate-dependent (and exhibit dynamical hysteresis). Systems in the previous category possess several properties, perhaps the most appealing is the emergence of scaling laws that relate the area enclosed of the hysteresis loop with the frequency, ω, and amplitude of a periodic driving force; the way in which ω and the external input relate to each other, and the value of the exponents of the scaling laws varies for every system (there is no universal behavior).

Scaling laws have been found in several systems exhibiting dynamical hysteresis, for example, a Langevin three-dimensional (3D) spin model subject to an external magnetic field [25] and a switched semiconductor laser [26]. Monte Carlo simulations in a two-dimensional (2D) model have

found that the scaling law exponents vary according to the systems dimension [27]; this has been verified using renormalization methods [28], suggesting that the difference between exponents is defined by the universality class to which the system belongs [29]. The noise intensity has major significance in the functional form of the scaling law behavior, as has been proven for a Ginzburg-Landau potential [30].

The article is organized as follows. In Sec. II we lay the groundwork for our electrochemical model by means of the Onsager's nonequilibrium thermodynamics; this scheme allows us to relate the concentrations in each electrode with the current for a supercapacitor. Our approach is consistent with the Butler-Volmer equation. In Sec. III we develop our model further in order to obtain a stochastic equation for the current, from which we were able to integrate in order to reproduce hysteresis cycles observed in experimental data. In Sec. III as a consequence that our model exhibits dynamical hysteresis, we obtained an expression for the entropy production per cycle. Last, we present our conclusions.

II. IRREVERSIBLE THERMODYNAMICS OF AN ELECTROCHEMICAL CELL

The current-overpotential equation relates the electrical current I in a electrochemical cell with the overpotential η of the electrode surface [31]. The standard procedure for deducing this equation is based on the theory of rate processes [32] and has the following form [31,33]:

$$I = I_c - I_a = I_0\left[\frac{c^{\rm ox}}{c^{\rm ox}_{\rm eq}}e^{-\alpha n\frac{F\eta}{RT}} - \frac{c^{\rm red}}{c^{\rm red}_{\rm eq}}e^{(1-\alpha)n\frac{F\eta}{RT}}\right]. \quad (1)$$

Here the cathodic and anodic electrical currents are indicated by I_c and I_a and the exchange current is defined as [31,33]

$$I_0 \equiv nAFk_0c_{\rm ox}^{(1-\alpha)}c_{\rm red}^{\alpha}, \quad (2)$$

where n is the number of electrons involved in the electrode reaction, A is the area of the electrode, F the Faraday's constant and k_0 the standard rate constant; α is known as the transference coefficient. The terms in the parentheses of Eq. (1) include the nonequilibrium concentrations of the compounds participating in the redox reaction taking place at the anode (ox) and the cathode (red), $c^{\rm ox}$ and $c^{\rm red}$, respectively, and their equilibrium counterparts $c^{\rm ox}_{\rm eq}$ and $c^{\rm red}_{\rm eq}$. The electrical energy associated with the overpotential, $F\eta$, is normalized with the thermal energy RT, with R the universal gas constant and T the temperature. When the nonequilibrium ion concentrations $c^{\rm ox}$ and $c^{\rm red}$ deviate weakly from their equilibrium values, $c^{\rm ox}/c^{\rm ox}_{\rm eq} \approx 1 \approx c^{\rm red}/c^{\rm red}_{\rm eq}$, the current-overpotential equation reduces to the commonly known Butler-Volmer equation, which is valid in the low current limit [31,33]. The Butler-Volmer equation obeys two limiting behaviors: (1) for large overvoltage values it reproduces the Tafel equation and (2) the Ohm law for small values of the overvoltage [34].

It was recently shown that the framework of nonequilibrium thermodynamics allows us to give a unified description of electrochemical processes since it establishes the basis to deduce both the Butler-Volmer and the Nernst equations over the same thermodynamics principles [35]. Here we benefit from this fact in order to formulate our more general model.

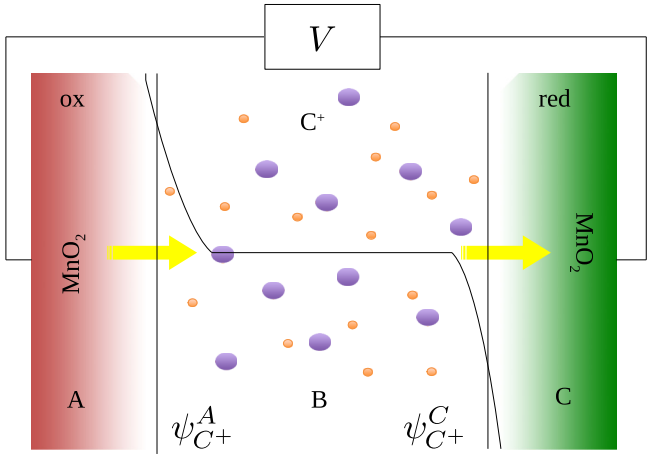

FIG. 1. Schematic representation of a symmetric supercapacitor.

A. Electrochemical affinity for a cell under nonequilibrium conditions

The most basic thermodynamic analysis of an electrochemical cell can be formulated by considering that the system has three regions: two regions corresponding to the surface of the electrodes, the anode A and the cathode C, and a third region, B, that is constituted by the ion solution (see Fig. 1).

Our goal in this section is to deduce the kinetic equation associated with the charge exchange per unit time at the surface of the electrodes. Hence, we are compelled to calculate the entropy production per unit time, d_iS/dt, of this process. This quantity satisfies the second law of thermodynamics, which is the most general criterion for the evolution of irreversible thermodynamic processes.

Thus, the total change of the entropy can be written, respectively, by the relations [36,37]

$$dS^A = d_eS^A + d_iS^A \quad \text{and} \quad dS^C = d_eS^C + d_iS^C \quad (3)$$

and

$$dS^B = d_eS^B + d_iS^B, \quad (4)$$

where the subindex e stands for the exchange of entropy with the surroundings and the subindex i for the entropy produced in the corresponding system due to irreversible processes. The total change of entropy is therefore given by

$$dS = dS^A + dS^B + dS^C. \quad (5)$$

Let us assume that the during operation the entropy exchanged between the electrodes and the solution is reversible so that d_eS^A, d_eS^B, and d_eS^C satisfy the relation $d_eS^A + d_eS^C = -d_eS^B$. If in a first approximation we make the assumption that the relevant irreversible processes taking place during the operation of the supercapacitor are due to the oxidation and reduction reactions taking place at the surface of the electrodes, that is, that diffusion across the solution does not contribute appreciably. Then we have that for the oxidation and reduction reactions in the anode $d_iS^A > 0$ and cathode $d_iS^C > 0$, whereas in region B, $d_iS^B \simeq 0$. In view of these

considerations, the total entropy change is simply given by

$$dS = d_i S^A + d_i S^C. \tag{6}$$

Our analysis may be generalized in order to consider other irreversible processes like ion diffusion in and between both regions or heat exchange along lines similar to those of Refs. [38,39]. Nevertheless, in this work we want to emphasize how the current-overpotential and the Butler-Volmer equations are naturally generalized when adopting a thermodynamic consistent approach, as well as the consequences of this generalization. Thus, we will restrict our analysis to analyze electrochemical reaction taking place at the surface of the working electrodes.

If the system operates at constant pressure and temperature, then the total entropy production ($d_i S = d_i S^A + d_i S^C$) and the Gibbs free energy are related by the well-known expression [40] $T d_i S = -dG \geqslant 0$. When the irreversible processes taking place in the system are the oxidation-reduction electrochemical reactions, then we may write

$$-T d_i S = dG^A + dG^C = \left[\sum_i^k \nu_i^A \tilde{\mu}_i^A + \sum_j^l \nu_j^C \tilde{\mu}_j^C \right] d\xi, \tag{7}$$

where k and l denote the total number of species and we have introduced the extent of reaction ξ, defined by the usual relation: $d\xi = dn_i/\nu_i$. Here n_i is mole number of the ith species taking place in the reaction and ν_i its corresponding stoichiometric coefficient, which follows the standard sign convention ($\nu_i > 0$ for products and $\nu_i < 0$ for reactants) [40].

The electrochemical potential $\tilde{\mu}_i$ is defined by the formula

$$\tilde{\mu}_i = \mu_i + z_i F \psi_i, \tag{8}$$

where ψ_i is the electrostatic potential of the ith ionic species with z_i its electrovalency and F the Faraday constant. In addition, the chemical potential, μ_i, is defined according to the well-known relation

$$\mu_i = \mu_i^0 + RT \ln |a_i|, \tag{9}$$

where μ_i^0 is the standard reference chemical potential, a_i, is the chemical activity that depends on the mole fractions of the chemical reagents, $x_i \equiv \frac{c_i}{c_\ominus}$, with c_i the concentration of the ith species and $c_\ominus$ is the standard amount of concentration. The activity can be written in the form

$$a_i(x_i) = x_i \gamma_i(x_i), \tag{10}$$

where the activity coefficient $\gamma_i(x_i)$ introduces all the nonidealities associated with the physical nature of the species participating in the electrochemical reaction and, more importantly, it should include nonidealities arising from the interaction between the ions and the surfaces of the electrodes and the electric double layer, to mention some effects. This point highlights the fact that the introduction of the activities a_i is unavoidable in order to propose a consistent thermodynamic model of the operation of systems like supercapacitors and even in the case of insertion batteries. An explicit relation between the chemical reagent mole fractions x_i and the extent of reaction ξ will be given in the next section.

Equation (7) can be written in terms of the electrochemical affinity

$$\tilde{\mathcal{A}} \equiv -\left[\sum_i^k \nu_i^A \tilde{\mu}_i^A + \sum_j^l \nu_j^C \tilde{\mu}_j^C \right], \tag{11}$$

which is the thermodynamic force driving the irreversible process associated with the chemicals reactions in each electrode. These reactions may be explicitly written as follows:

$$\begin{aligned} \text{C}: &\quad \sum_i \nu_i^C X_i^C + \text{ne}_C^- \rightleftharpoons \sum_i \nu_i^C X_{\text{red},i}^C, \\ \text{A}: &\quad \sum_j \nu_j^A Y_j^A \rightleftharpoons \sum_j \nu_j^A Y_{\text{ox},j}^A + \text{ne}_A^-, \end{aligned} \tag{12}$$

where n is the number of electrons transferred in the chemical reaction. The total electrochemical reaction reads

$$\begin{aligned} &\sum_i \nu_i^C X_i^C + \sum_j \nu_j^A Y_j^A + \text{ne}_C^- \\ &\quad \rightleftharpoons \sum_i \nu_i^C X_{\text{red},i}^C + \sum_j \nu_j^A Y_{\text{ox},j}^A + \text{ne}_A^-. \end{aligned} \tag{13}$$

The electrochemical affinity can be explicitly expressed by means of Eq. (11) and is given by

$$\begin{aligned} \tilde{\mathcal{A}} = &\sum_i \nu_i^C \tilde{\mu}_{X,i}^C + \sum_j \nu_j^A \tilde{\mu}_{Y,j}^A + n\tilde{\mu}_e^C \\ &- \sum_i \nu_i^C \tilde{\mu}_{\text{Xred},i}^C - \sum_j \nu_j^A \tilde{\mu}_{\text{Yox},j}^A - n\tilde{\mu}_e^A. \end{aligned} \tag{14}$$

Equation (14) can be further simplified with the substitution of Eqs. (8)–(10). Using the properties of the logarithms and collecting terms the resulting expression is

$$\begin{aligned} \tilde{\mathcal{A}} = &-\Delta G_0 - nF\mathcal{E} + RT\left[\ln\left| \frac{a_C^{\text{ox}}}{a_C^{\text{red}}} \right| - \ln\left| \frac{a_A^{\text{ox}}}{a_A^{\text{red}}} \right| \right] \\ &+ F \sum_{q=C}^{A} \left[\sum_i z_i^q \nu_i^q \psi_i^q - \sum_j z_j^q \nu_j^q \psi_j^q \right]. \end{aligned} \tag{15}$$

The first term of this equation is the standard Gibbs free energy: $\Delta G_0 \equiv \sum_q \sum_r \nu_r \mu_r^{0,q}$, where the subindex r represents the contributions of all reagents at the electrolyte of both reactants and products and $q = A, C$. The second term is the whole cell potential difference: $\mathcal{E} \equiv \psi_C - \psi_A$. The last terms of Eq. (15) contain the activities associated with oxidation a_q^{ox} and reduction a_q^{red} reactions in both electrodes which were defined according to the relations

$$\begin{aligned} &a_C^{\text{ox}} = \prod_i a_{X,i}^{\nu_i^C}, \quad a_A^{\text{red}} = \prod_j a_{Y,j}^{\nu_j^A}, \\ &a_C^{\text{red}} = \prod_i a_{\text{Xred},i}^{\nu_i^C} \quad \text{and} \quad a_A^{\text{ox}} = \prod_j a_{\text{Yox},j}^{\nu_j^A}. \end{aligned} \tag{16}$$

The last term in Eq. (15) represent the electrical potential of the reagents at the electrolyte and can be used to describe, for instance, cations near a double layer or in a nonhomogeneous electrolyte (in which bulk potential is not uniform). The splitting into sums over indexes i and j explicitly takes

into account the sign convention of the stoichiometric coefficients of products (i) and reagents (j). In equilibrium, or near equilibrium, all chemical species in the electrolyte are at the same bulk potential, so $\psi_b = \psi_r^q$. Therefore, the corresponding sum of the electrical potentials satisfies the relation $\sum_{q,r} z_r^q \nu_r^q \psi_r^q = \psi_b \sum_{q,r} z_r^q \nu_r^q = 0$, which vanishes because the whole electrolyte, and the reagents in it, are at electrochemical equilibrium. This assumption is consistent with our previous assumptions on the entropy production of the electrolyte (region B) also vanishes.

In equilibrium, the electrochemical affinity (15) vanishes, $\mathcal{E} = \mathcal{E}_{\rm eq}$, and therefore we may write

$$\mathcal{E}_{\rm eq} = \mathcal{E}_0 - \frac{RT}{nF}\left[\frac{a_{C,\rm eq}^{\rm ox} a_{A,\rm eq}^{\rm red}}{a_{C,\rm eq}^{\rm red} a_{A,\rm eq}^{\rm ox}}\right], \tag{17}$$

where we have introduced the equality $\Delta G_0 = -nF\mathcal{E}_0 = -nF(\mathcal{E}_0^C - \mathcal{E}_0^A)$ and the equilibrium activities $a_{i,\rm eq}$. The last equation is the classical Nernst equation for the equilibrium potential.

B. Generalization of the current-overpotential equation

In this subsection, we will derive the current-overpotential equation for the half-cell reaction occurring at the cathode and finish our general analysis showing the consistency of the theoretical approach used with well-known results of the literature in the corresponding limiting cases.

The entropy production at the cathode appearing in Eq. (7) can be rewritten in the form

$$-\frac{dG^C}{dt} = \frac{\tilde{\mathcal{A}}^C}{T}\frac{d\xi}{dt} = \frac{\tilde{\mathcal{A}}^C}{T} J_\xi > 0, \tag{18}$$

where $J_\xi \equiv d\xi/dt$ and the electrochemical affinity $\tilde{\mathcal{A}}^C$ at the cathode is given by

$$\tilde{\mathcal{A}}^C = -\Delta G_0^C + RT \ln a_C^{\rm ox} - RT \ln a_C^{\rm red} - nF\mathcal{E}^{\mathcal{C}}, \tag{19}$$

with $\Delta G_0^C = \sum_r \nu_r \mu_r^{0,C}$ and the cathode potential given by $\mathcal{E}^C = \psi^C$. Since the entropy production must be a positive quantity in accordance with the second law of thermodynamics, we may follow the postulates of nonequilibrium thermodynamics and assume that that fluxes and forces are proportional to each other with an Onsager coefficient as a proportionality coefficient [40,41]. Hence, we may write [42]

$$J_\xi = \beta \tilde{\mathcal{A}}(\xi), \tag{20}$$

where β is an Onsager coefficient with units $[\beta^{-1}] = \mathrm{J\,s/mol}$ and may, in general, be a function of the state variables like the temperature T, the chemical activities $a(x)$, and the electric potential ψ [40].

The load-voltage equation (20) connects the evolution of the extent of reaction ξ, that measures the loading state of the electrodes as the electrochemical reaction advances, with the voltage. Solving this equation allows to obtain the time evolution of $\xi(t)$.

Now, taking into account that the electrical current is related to the number of faradays transferred at the electrodes and the reaction velocity [2,41], we may define the electrical current as

$$I \equiv q_{tr} k_0 \frac{\tilde{\mathcal{A}}}{RT}, \tag{21}$$

where q_{tr} represents the effective amount of charge transferred at the electrodes and, for convenience, we have written $\beta = k_0/RT$ with k_0 the reaction velocity constant. Using Eq. (19) in Eq. (21) we obtain the following general expression for the electrical current:

$$\frac{I}{I_{tr}} = \frac{-\Delta G_0^{\mathcal{C}}}{RT} + \ln\left[\frac{a_C^{\rm ox} e^{-nF\mathcal{E}^{\mathcal{C}}/RT}}{a_C^{\rm red}}\right], \tag{22}$$

where we have defined the effective transference current $I_{tr} = q_{tr} k_0$. Now, using the relation $\mathcal{E}_0^{\mathcal{C}} = -\Delta G_0^{\mathcal{C}}/nF$ the last formula transforms into

$$\frac{I}{I_{tr}} = \ln\left[\frac{a^{\rm ox}}{a^{\rm red}} e^{-\frac{nF(\mathcal{E}-\mathcal{E}_0)}{RT}}\right], \tag{23}$$

where we have dropped the superscript $\mathcal{C}$ for notation simplicity. The explicit dependence of the rate constant k_0 on temperature and other variables may be determined from a microscopic theory, like the theory of absolute reaction rates and its generalizations to the case of electron transfer in the presence of quantum effects; see Refs. [32,43].

Equation (23) can be written in a more familiar way by splitting the exponential after introducing the charge transference coefficient α, which measures the fraction of the interfacial potential between the electrode and the electrolyte [31]. Thus, we may write

$$\frac{I}{I_{tr}} = \ln\left[\frac{a^{\rm ox}}{a^{\rm red}} \frac{e^{-\alpha\frac{nF(\mathcal{E}-\mathcal{E}_0)}{RT}}}{e^{(1-\alpha)\frac{nF(\mathcal{E}-\mathcal{E}_0)}{RT}}}\right]. \tag{24}$$

Equation (24) represents the most general way to express the electrical current associated to an heterogeneous oxidation-reduction reaction and is fully consistent with the Nernst equation when equilibrium is reached.

The current-overpotential equation and the Butler-Volmer equation are particular cases of Eq. (24), which are valid for ideal systems near equilibrium. This can be shown by writing Eq. (24) in the more convenient form

$$\frac{I}{I_{tr}} = \ln\left[a^{\rm ox} e^{-\alpha\frac{nF(\mathcal{E}-\mathcal{E}_0)}{RT}}\right] - \ln\left[a^{\rm red} e^{(1-\alpha)\frac{nF(\mathcal{E}-\mathcal{E}_0)}{RT}}\right]. \tag{25}$$

Introducing now the equilibrium potential difference $\mathcal{E}_q$, Eq. (25) becomes

$$\frac{I}{I_{tr}} = \ln\left[a^{\rm ox} e^{-\alpha\frac{nF(\mathcal{E}-\mathcal{E}_q+\mathcal{E}_q-\mathcal{E}_0)}{RT}}\right] - \ln\left[a^{\rm red} e^{(1-\alpha)\frac{nF(\mathcal{E}-\mathcal{E}_q+\mathcal{E}_q-\mathcal{E}_0)}{RT}}\right]. \tag{26}$$

A first order expansion of the logarithms around the equilibrium value of their arguments [$\ln x \sim (x-1) + O(x^2)$] yields

$$\frac{I}{I_{tr}} = a^{\rm ox} e^{-\alpha\frac{nF(\mathcal{E}-\mathcal{E}_q)}{RT}} e^{-\alpha\frac{nF(\mathcal{E}_q-\mathcal{E}_0)}{RT}} - a^{\rm red} e^{(1-\alpha)\frac{nF(\mathcal{E}-\mathcal{E}_q)}{RT}} e^{(1-\alpha)\frac{nF(\mathcal{E}_q-\mathcal{E}_0)}{RT}}. \tag{27}$$

Equation (27) can be simplified by identifying the overvoltage $\eta \equiv \mathcal{E} - \mathcal{E}_q$ and noticing that the exponentials carrying the term $\mathcal{E}_q - \mathcal{E}_0$ can be rewritten in terms of the equilibrium concentrations by means of the Nernst equation for the half-cell:

$$e^{-\frac{nF}{RT}(\mathcal{E}_q - \mathcal{E}_0)} = \frac{a^{\rm red}_{\rm eq}}{a^{\rm ox}_{\rm eq}}, \tag{28}$$

which was obtained from Eq. (19). Substituting now the relation (28) into Eq. (27) and making some rearrangements, we finally obtain the current-overpotential equation

$$\frac{I}{\tilde{I}_0} = \frac{a^{\rm ox}}{a^{\rm ox}_{\rm eq}} e^{-\alpha \frac{nF\eta}{RT}} - \frac{a^{\rm red}}{a^{\rm red}_{\rm eq}} e^{(1-\alpha)\frac{nF\eta}{RT}}, \tag{29}$$

where we have identified the generalized exchange current $\tilde{I}_0$:

$$\begin{aligned}\tilde{I}_0 &= I_{tr}\left[a^{\rm ox}_{\rm eq}\right]^{1-\alpha}\left[a^{\rm red}_{\rm eq}\right]^{\alpha} \\ &= nFAk_0[\gamma^{\rm ox}]^{1-\alpha}[\gamma^{\rm red}]^{\alpha}\left[c^{\rm ox}_{\rm eq}\right]^{1-\alpha}\left[c^{\rm red}_{\rm eq}\right]^{\alpha}.\end{aligned} \tag{30}$$

Comparison of this expression with ours suggests that the effective charge transferred is related with the the surface concentration of ions at the electrode, $c^{\ominus}$, and thus, in this limit it obeys the relation $q_{tr} = c^{\ominus} nFA$. The exchange current has been generalized in other works by including excluded volume effects [18] or by considering the electron transference process [20]. Here have neglected this second process because we assumed fast chemical kinetics. However, these and other effects can also be incorporated in our description.

The Butler-Volmer equation can be obtained from Eq. (29) in the low-current limit for ideal systems: $\gamma^q \simeq 1$ and $a^q/a^q_{\rm eq} \simeq c^q/c^q_{\rm eq} \simeq 1$ for $q = {\rm ox,red}$.

III. GENERALIZED CURRENT-OVERPOTENTIAL EQUATION FOR A MODEL REDOX-PSEUDOCAPACITOR

In this section we will formulate a minimal electrokinetic model describing the operation of an idealized redox-pseudocapacitor, understood as a pseudocapacitor whose time behavior is dominated by the chemical kinetics and not by diffusive transport processes [44,45].

Our analysis will follow the general scheme presented in previous section and focuses on the description of the charging or discharging process in terms of the extent of reaction ξ, which reflects the loading state of the capacitor in the following way. As the reaction advances, the extent of reaction evolves from a completely charged state to a fully discharged state. The different degrees of loading are represented by ξ, with $\xi \in [0,1]$. Here $\xi = 1$ represents the charged state and $\xi = 0$ the discharged state. The value of the extent of reaction depends upon the chemical affinity of the reaction and the external voltage and is, in general, influenced by fluctuations in chemical reagents at the surface of the electrodes.

The modeling of the charging or discharging process is carried out in terms of a reversible chemical reaction which is the sum of the half-reactions in each electrode. Let us consider a MnO_2-based pseudocapacitor. In this case the charging or discharging process happens through a redox reaction in which the Mn changes its oxidation state from +4 to +3 by the following reversible reactions [3,46]. At the cathode we have

$$\rm C: \quad [MnO_2]^C + C^+ + e^- \rightarrow [MnO_2^- C^+]^C, \tag{31}$$

where C^+ stands for an alkali cation that may be Na^+, Li^+, or K^+. Due to the fact that most capacitors are made with symmetrical electrodes, we assume that the other electrode follows a similar reaction but with the peculiarity that the extent of reaction advances in the opposite direction

$$\rm A: \quad [MnO_2^- C^+]^A \rightarrow MnO_2^A + C^+ + e^-. \tag{32}$$

Thus, the complete electrochemical reaction is

$$\begin{aligned}&[{\rm MnO_2}]^C + [{\rm MnO_2^- C^+}]^A + C^+ + e_A^- \\ &\quad \rightleftharpoons [{\rm MnO_2^- C^+}]^C + [{\rm MnO_2}]^A + C^+ + e_C^-.\end{aligned} \tag{33}$$

The electrochemical affinity for the complete cell reaction can be expanded by means of Eq. (11) and by following the standard sign convention [47], then reads

$$\begin{aligned}\tilde{\mathcal{A}} = &\tilde{\mu}^C_{\rm MnO_2} + \tilde{\mu}^A_{\rm MnO_2^- C^+} + \tilde{\mu}^C_{\rm C^+} + \tilde{\mu}^C_e \\ &- \tilde{\mu}^C_{\rm MnO_2^- C^+} - \tilde{\mu}^A_{\rm MnO_2} - \tilde{\mu}^A_{\rm C^+} - \tilde{\mu}^A_e.\end{aligned} \tag{34}$$

The electrochemical potentials appearing in Eq. (34) can be expanded by using Eq. (8). Considering now that the anode and the cathode are at fixed given potentials, then the following equalities hold: $\psi^A_{\rm MnO_2^- C^+} = \psi^A_{\rm MnO_2}$ and $\psi^C_{\rm MnO_2} = \psi^C_{\rm MnO_2^- C^+}$. In the case of the chemical potentials we have the equalities $\mu^A_e = \mu^C_e$ and $\mu^C_{\rm MnO_2} = \mu^A_{\rm MnO_2}$ due to the fact that they represent the same material at identical proportions.

Using these relation into Eq. (34) we obtain that the electrochemical affinity reduces to

$$\begin{aligned}\tilde{\mathcal{A}} = &-\mathcal{A}_0 + \mu^A_{\rm MnO_2^- C^+} + \mu^C_{\rm C^+} - \left[\mu^C_{\rm MnO_2^- C^+} + \mu^A_{\rm C^+}\right] \\ &- F\psi^C + F\psi^A + F\psi^C_{\rm C^+} - F\psi^A_{\rm C^+}.\end{aligned} \tag{35}$$

The ion concentrations at the reaction plane can be written in terms of the bulk concentrations by following the Frumkin approach [48]. Hence, we use the Poisson-Boltzmann ion distribution [23], which reads

$$\begin{aligned}c^C_{\rm C^+} &= c_{\rm bulk} e^{-F(\psi^C_{\rm C^+} - \psi_{\rm bulk})/RT}, \\ c^A_{\rm C^+} &= c_{\rm bulk} e^{-F(\psi_{\rm bulk} - \psi^A_{\rm C^+})/RT}.\end{aligned} \tag{36}$$

Similarly, each chemical potential at the reaction plane can now be written in the following manner:

$$\begin{aligned}\mu^C_{\rm C^+} &= RT \ln \gamma^+ c_{\rm bulk} e^{-F(\psi^C_{x\rm C^+} - \psi_{\rm bulk})/RT} \\ \mu^A_{\rm C^+} &= RT \ln \gamma^+ c_{\rm bulk} e^{-F(\psi_{\rm bulk} - \psi^A_{\rm C^+})/RT}.\end{aligned} \tag{37}$$

Substituting Eq. (37) into Eq. (35) and following the results of the previous section we have that the electrochemical affinity reduces to

$$\tilde{\mathcal{A}} = RT \ln \left[\frac{a^A_{\rm MnO_2^- C^+}}{a^C_{\rm MnO_2^- C^+}}\right] - \kappa F(\mathcal{E} - \mathcal{E}_0), \tag{38}$$

where we have introduced the effective charge transfer coefficient $\kappa \in [0,1]$ measuring the effectiveness of charge transfer in the electrokinetic reactions.

A. Mass fractions, activities, and extent of reaction

During the charging or discharging process of the supercapacitor the composition of each electrode changes as the reaction evolves. When the supercapacitor is fully charged, the anode composition is $MnO_2^-C^+$. As the reaction advances, its composition changes until the anode composition is MnO_2. In a similar way, the cathode composition changes from MnO_2 to $MnO_2^-C^+$.

In view of this, the anode and cathode activities in Eq. (38) can be modeled by considering that the compound $[MnO_2^-C^+]^{A,C}$ can be described as a solid mixture of the pure substances MnO_2 and $MnO_2^-C^+$. Thus, although the state of composition represented by the number of moles $n_{[MnO_2^-C^+]^{A,C}}$ of $[MnO_2^-C^+]^{A,C}$ at the anode and the cathode varies as the reaction advances, the total number of moles n_T of the pure quantities MnO_2 and $MnO_2^-C^+$ remains constant during the whole charging or discharging process:

$$n_T = n_{MnO_2} + n_{MnO_2^-C^+}. \tag{39}$$

The molar fractions which represent the composition of each electrode during the charging or discharging process can be defined as

$$x^A_{MnO_2^-C^+} = \frac{n_{[MnO_2^-C^+]^A}}{n_T},$$
$$x^C_{MnO_2^-C^+} = \frac{n_{[MnO_2^-C^+]^C}}{n_T}. \tag{40}$$

If the initial state of the supercapacitor corresponds to the discharged state, each molar number can be written in terms of the extent of reaction according to the relations

$$n_{[MnO_2^-C^+]^A} = \xi n_T \quad \text{and} \quad n_{[MnO_2^-C^+]^C} = (1-\xi)n_T. \tag{41}$$

Thus, the molar fractions are given by

$$x^A_{MnO_2^-C^+} = \xi \quad \text{and} \quad x^C_{MnO_2^-C^+} = 1-\xi \tag{42}$$

and obey the relation

$$x^A_{MnO_2^-C^+} + x^B_{MnO_2^-C^+} = 1. \tag{43}$$

Recalling Eq. (10), the anode and cathode activities in Eq. (38) can now be written in the form

$$a^A_{MnO_2^-C^+} = x^A_{MnO_2^-C^+}\gamma^A_{MnO_2^-C^+},$$
$$a^C_{MnO_2^-C^+} = x^C_{MnO_2^-C^+}\gamma^C_{MnO_2^-C^+}, \tag{44}$$

where the activity coefficients $\gamma^{A,C}_{MnO_2^-C^+}$ account for the deviation of the system with respect to the diluted case.

Since both activity coefficients $\gamma^{A,C}_{MnO_2^-C^+}$ change as the reaction advances, then they must depend on the extent of reaction. However, this dependence must be consistent with the limiting behavior of pure substances $\gamma_{MnO_2^-C^+}$ and γ_{MnO_2}; that is, when the supercapacitor is fully charged the anode composition is $MnO_2^-C^+$, and when it is fully discharged its composition is MnO_2. The inverse conditions apply for the cathode.

The corresponding limiting behaviors for each activity coefficient can be reproduced by using the Vegard law [49], which relates the limiting states by means of the following the linear relation in terms of the extent of reaction

$$\ln\gamma^A_{MnO_2^-C^+} = (1-\xi)\ln\gamma_{MnO_2^-C^+} + \xi\ln\gamma_{MnO_2},$$
$$\ln\gamma^C_{MnO_2^-C^+} = \xi\ln\gamma_{MnO_2^-C^+} + (1-\xi)\ln\gamma_{MnO_2}, \tag{45}$$

where $\gamma_{MnO_2^-C^+}$ and γ_{MnO_2} are the pure substance activity coefficients. Vegard's law is commonly used to model the volume change in solid mixtures [50] and can be generalized to other properties; see Ref. [51]. Equations (45) allow us to describe both the charged and discharged states with $\xi = 0$ and $\xi = 1$, respectively.

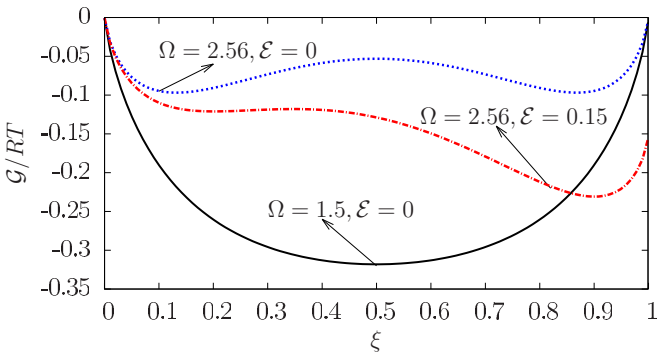

FIG. 2. Schematic comparison between three characteristic curves of Gibbs free energy.

B. Load-voltage and current-voltage equations

The results of the previous paragraph allow us to write the electrochemical affinity in terms of the extent of reaction. Substituting Eqs. (42) and (45) into Eq. (44) and the result into Eq. (38), the electrochemical affinity then becomes

$$\tilde{\mathcal{A}}(\xi) = RT\left[\ln\left(\frac{\xi}{1-\xi}\right) - \Omega(1-2\xi)\right] - \kappa F(\mathcal{E}-\mathcal{E}_0), \tag{46}$$

where the regular parameter is defined in terms of the activity coefficients of the pure substances by the relation $\Omega = \ln|\gamma_{MnO_2}/\gamma_{MnO_2^-C^+}|$. It is convenient to notice that the use of Vegard's law leads to an expression of the chemical part of the affinity which is entirely similar to a regular mixture expression. This fact suggests that, if the linear relation between limiting states of the Vegard's law is replaced by a nonlinear relation, then a more general expression for the affinity can be obtained. This will be studied in future work. The regular parameter can be related to the height of the energy barrier by integrating the electrochemical affinity, by means of Eq. (7), in order to obtain

$$G(\xi) = RT[(1-\xi)\ln(1-\xi) + \xi\ln\xi + \Omega(1-\xi)\xi + \epsilon\mathcal{E}_c\xi] + G_0, \tag{47}$$

where $\mathcal{E}_c$ stands for a fixed voltage, G_0 is an integration constant, and $\epsilon = \kappa F/RT$. Figure 2 shows how the regular parameter Ω controls the height of the free energy barrier in Eq. (47). By increasing the nonideality yields a higher barrier.

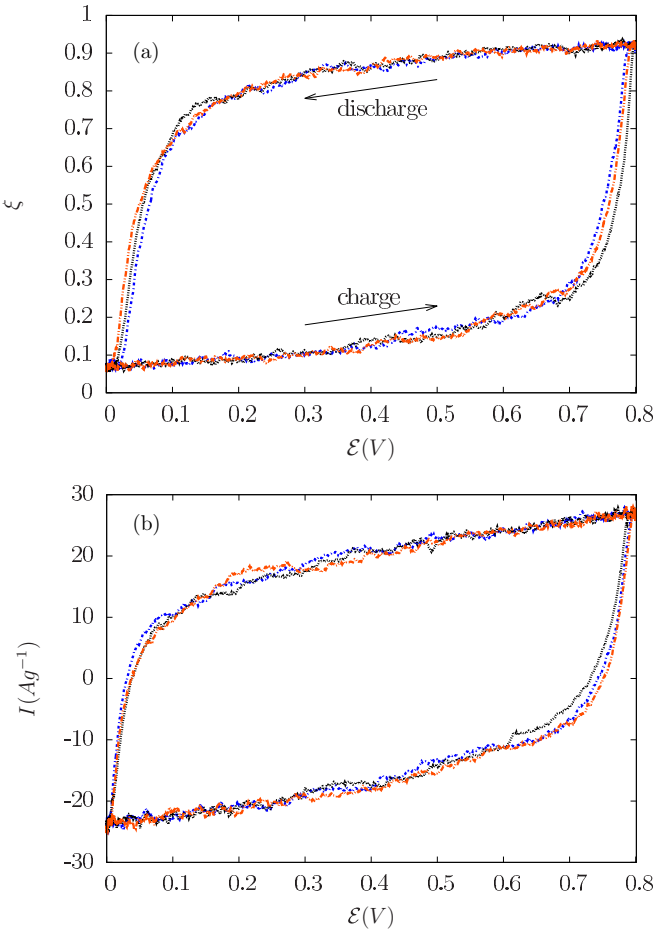

FIG. 3. (a) Three overlapping Langevin trajectories for fixed values $\mathcal{E}_1 = 0.4\,\mathrm{V}$, $\Omega = 2.56$, $\omega = 0.2748\,\mathrm{s}^{-1}$, $k_0 = 0.077\,\mathrm{s}^{-1}$, and $\kappa = 0.025$. (b) Three overlapping voltagrams for the same parameters.

The substitution of Eq. (46) into Eq. (20) yields the general load-voltage equation

$$\frac{d\xi}{dt} = k_0\left[\ln\left(\frac{\xi}{1-\xi}\right) - \Omega(1-2\xi) - \frac{\kappa F}{RT}(\mathcal{E}-\mathcal{E}_0)\right] + \zeta(t). \tag{48}$$

Here, for completeness, we have included the presence of thermal fluctuations in the system through the term $\zeta(t)$ accounting for the fluctuations of the concentrations of the reacting species at each electrode. We will assume that these fluctuations are thermal, that is, they are characterized by a white noise with zero mean and correlation function given by $\langle\zeta(t)\zeta(t')\rangle = 2k_bTk_0\delta(t-t')$.

A numerical solution of Eq. (48) for $\xi(t)$ can be computed by first expanding the logarithmic terms by using a (8,8)-th order Padè approximant and solving for each voltage by means of the Euler-Maruyama method [52].

Figure 3(a) shows some numerical solutions for the extent of reaction, $\xi(t) = \xi[\mathcal{E}(t)]$, as a function of the applied voltage, $\mathcal{E}(t)$, which for simplicity is given by an oscillating function of the form $\mathcal{E}(t) = \mathcal{E}_1\sin(\omega t)$, with ω a characteristic angular frequency.

When the obtained data are substituted into the expression for the electrochemical affinity $\tilde{\mathcal{A}}(\xi)$ in Eq. (46), and the result into Eq. (21), then one obtains the general fluctuating current-voltage relation

$$\frac{I}{I_\rho} = \ln\left[\frac{\xi(t)}{1-\xi(t)}\right] - \Omega[1-2\xi(t)] - \kappa\frac{F[\mathcal{E}(t)-\mathcal{E}_0]}{RT}. \tag{49}$$

Here the current density is defined as $I_\rho \equiv q_{tr}k_0/m$ (Ag^{-1}), with m the mass of the active materials at the electrodes. In Fig. 3(b) we show the typical voltagrams obtained from Eq. (49). As expected, the current-voltage plot shows the hysteresis of the system during a charge or discharge process.

Notwithstanding that a detailed analysis and interpretation of Figs. 3(a) and 3(b) for an specific case will be provided in the next section, it is worth stress that the three Langevin trajectories calculated during one cycle, shown in Fig. 3(a), indicate that the behavior of the supercapacitor can be interpreted as the average of those trajectories. During the process of loading and unloading of the electrodes, the external potential changes in a continuous manner, meaning that an arbitrary state of loading depends on the noise intensity and the rate at which the external voltage changes. Hence, Eq. (48) implies that a very fast chemical kinetics is taking place at the electrodes, in such a way that any sudden change in the external voltage induces an instantaneous change in the extent of reaction.

IV. COMPARISON WITH EXPERIMENTS

The behavior of a supercapacitor may emerge from several coupled physical phenomena. For instance, in the cases when ion insertion in the electrodes is important, it could induce a volume change of the electrodes. This effect would imply that the electrochemical phenomena can be coupled with the ion insertion through the lattice crystal of the electrode and, therefore, with surface and bulk-transport effects through the pores of the crystal. Thus, in the general case both contributions to the current must be taken into account. Nonetheless, if the loading-unloading process occurs very fast for certain classes of electrodes, it is reasonable to assume that the charging-discharging kinetics is surface-controlled (capacitive) and, therefore, it is valid to neglect insertion and diffusive contributions to the current behavior.

In practice this can be evaluated by means of cyclic voltametric experiments, since the functional relation between the current and the sweep rate ν (Vs^{-1}) can be used to discern among surface and diffusion controlled processes [53] and therefore to determine for which systems and conditions the insertion and diffusive effects can be neglected.

Here we will compare theory with experiments for a MnO_2-based supercapacitor with small current density under the assumption that a very fast chemical kinetics controls its behavior.

The comparison can be done by first generating an ensemble of simulation data for $\xi(t)$ after solving the load-voltage equation (48) and then calculating the mean value of the extent of reaction, $\bar{\xi}[\mathcal{E}(t)]$. Then, following the steps indicated in the previous section, one may derive the averaged current-voltage

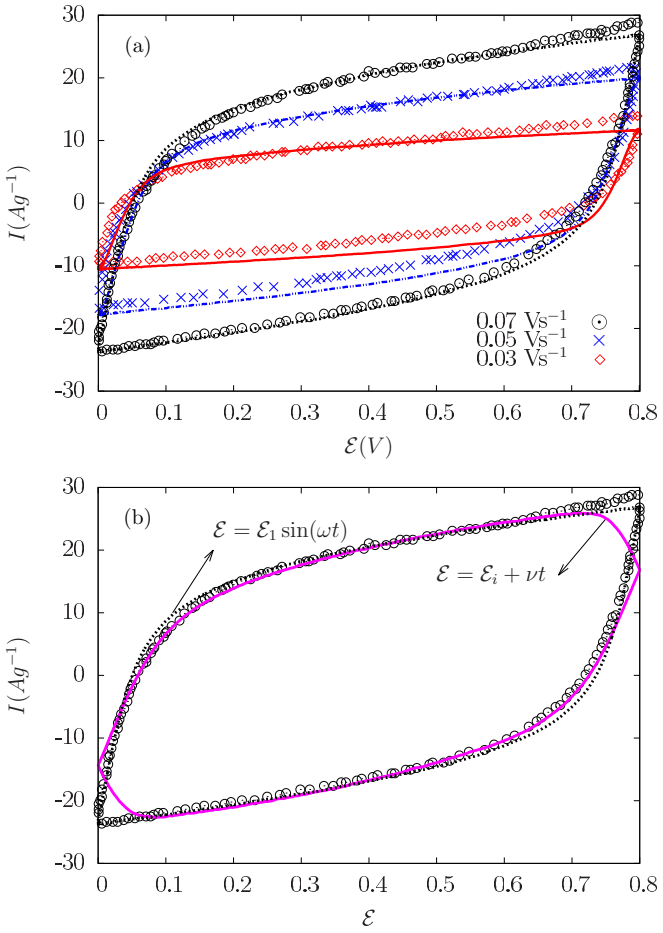

FIG. 4. Experimental data fitting of the CV with sweep rates $\nu = 0.03$ Vs^{-1} (diamons), $\nu = 0.05$ Vs^{-1} (crosses), and $\nu = 0.07$ Vs^{-1} (circles) with the parameters given in the text. (b) Comparision of a experimental data fitting of a CV with sweep rate $\nu = 0.07$ Vs^{-1} (circles) by means of a sinosoidal (dots) and triangular (continuous line) voltage oscillation.

relation

$$\frac{I}{I_\rho} = \ln\left(\frac{\bar{\xi}}{1-\bar{\xi}}\right) - \Omega(1-2\bar{\xi}) - \frac{\kappa F}{RT}(\mathcal{E}-\mathcal{E}_0). \tag{50}$$

This equation was used to fit experimental cyclic voltagrams (CV) of a symmetrical supercapacitor; see Ref. [54]. The experimental CV curves correspond to electrodes based on MnO_2 spheres decorated by carbon-coated cobalt nanobeads (MnO_2-NPs@Co/C). Figure 4(a) shows the comparison between experiments and theory for an electrical potential window of 0–0.8 V and scan (sweep) rates of $\nu = 0.03$ Vs^{-1} (diamonds), 0.05 Vs^{-1} (crosses), and 0.07 Vs^{-1} (circles).

The lines were obtained by using Eq. (50) for two cyclic voltametric protocols corresponding to a periodic external potential of the form $\mathcal{E}(t) = \mathcal{E}_1 \sin(\omega t)$. The comparison using a sinusoidal protocol is acceptable in all cases [Fig. 4(a)] although the model works better for larger sweep rates. The Fig. 4(b) shows the comparison between the fits performed using sinusoidal (dotted line) and triangular protocols (solid line) for $\mathcal{E}(t)$. The results indicate that the experimental data has a softer voltage inversion (like that of the sinusoidal model); see the turning points of the current-voltage representation.

For the first case, $\nu = 0.03$ Vs^{-1} (diamonds) was fitted by using the parameters $I_\rho = 2$ Ag^{-1}, $\Omega = 2.75$. In the second case, $\nu = 0.05$ Vs^{-1} (crosses) was fitted with the parameters $I_\rho = 3.6$ Ag^{-1}, and $\Omega = 2.62$. Finally, with the third third case, $\nu = 0.07$ Vs^{-1} (circles), was fitted with $I_\rho = 4.95$ Ag^{-1}, and $\Omega = 2.56$. The values of the other parameters are $\kappa = 0.025$, $\mathcal{E}_1 = 0.4$ V, and $\mathcal{E}_0 = 0.4$ V. The difference between the regular parameters used to fit each CV curve shows a dependence of the activity coefficients with the sweep rate. We conjecture that the origin of this dependence may be found in the mechanical properties (elastic moduli) of the electrodes during operation. However, the description of this effect deserves a detailed study that goes beyond the regular model presented here.

V. ENERGY DISSIPATION AND ENTROPY PRODUCTION OF A PSEUDOCAPACITOR

One of the main features of batteries and supercapacitors that exhibit dynamical hysteresis is the dependence of the enclosed area with the angular frequency of the external voltage in such a way that, if ω increases then the area of the cycle increases, meaning a higher energy dissipation during cycling. The main consequence of the hysteresis translates into several technical difficulties in applications and imposes limits on the performance of these systems.

Thus, it is convenient to determine the dependence of the energy dissipation for the model we have proposed by analyzing its energy dissipation as a function of the voltage frequency ω, the regular parameter Ω determining the height of the free energy barrier associated with the electrochemical reaction and of the amplitude of the imposed voltage $\mathcal{E}$. These dependences can be deduced by using the first law of thermodynamics, which for this system reads

$$dU = \delta Q + \mathcal{E}(t)\, dq, \tag{51}$$

where $\mathcal{E}(t)\, dq$ represents the differential work provided by the external voltage $\mathcal{E}(t)$ to transfer the charge differential, dq. Then Eq. (51) can be substituted into the dissipated energy per cycle, given by

$$E_d = -\oint \delta Q = \oint (\mathcal{E}(t)\, dq - dU), \tag{52}$$

which can be further simplified by noticing that the internal energy U is a state function, that satisfies $\oint dU = 0$, in order to write

$$E_d = \oint \mathcal{E}(t)\, dq. \tag{53}$$

Taking into account Eqs. (20) and (21), we obtain $dq = q_{tr}\, d\xi$, and, therefore, we can identify the dissipated energy with the enclosed area, A_c, of the hysteresis cycle which satisfies the relation

$$\frac{E_d^\Omega}{\mathcal{E}_1 q_{tr}} = \oint \frac{\mathcal{E}(t)}{\mathcal{E}_1}\, d\xi = A_c(\omega, \Omega, \mathcal{E}_1), \tag{54}$$

where $\mathcal{E}_1 q_{tr}$ acts as a reference value of the energy. From Eq. (54) it follows that the energy dissipated has a strong

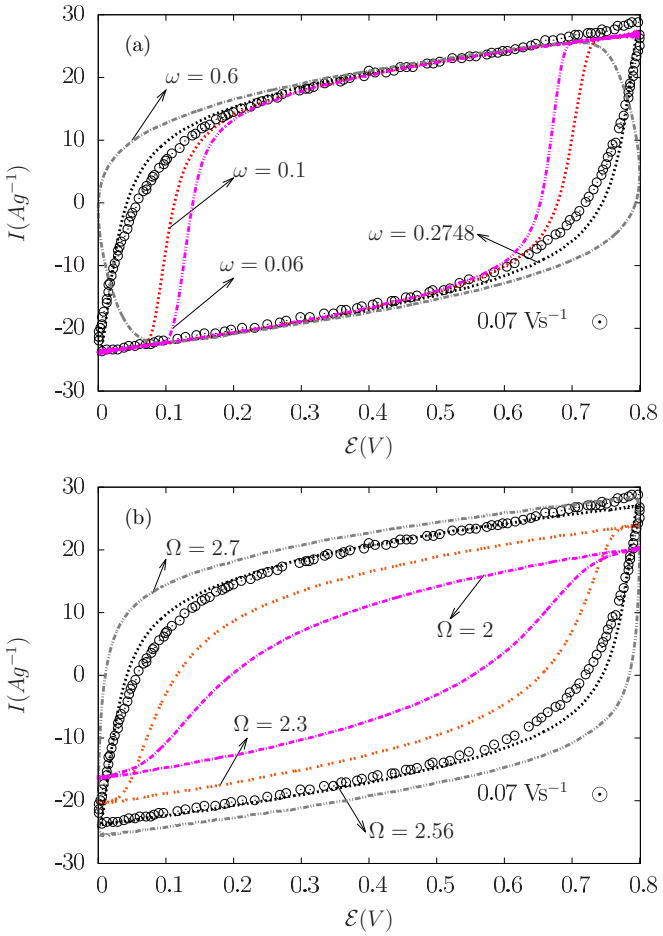

FIG. 5. Experimental data fitting for $\nu = 0.07\ \mathrm{Vs}^{-1}$ (circles) with parameters: $I_\rho = 4.95$, $\omega = 0.2748$, $\mathcal{E}_1 = \mathcal{E}_0 = 0.4$, $\kappa = 0.025$, $\zeta = 0.025$, and $\Omega = 2.56$. (a) Comparison of the fitting curves by fixing all parameters and changing ω. (b) Comparison of the fitting curves by fixing all parameters and changing Ω.

dependence on the external frequency ω, the height of the free energy barrier Ω and the amplitude of the external voltage applied $\mathcal{E}_1$.

In general, the dependence of the energy dissipated, or the cycle area $A_c(\omega)$ on the frequency ω of the externally applied voltage is nonmonotonic. Thus, for convenience we may introduce the maximum dissipated energy $E^{\Omega}_{d,\max}(\omega^{\Omega}_{\max})$ in order to normalize the results. Noticing that

$$\frac{E^{\Omega}_{d,\max}}{\mathcal{E}_1 q_{tr}} = A^{\Omega}_{c,\max}, \tag{55}$$

then we may write the general relation

$$\frac{E_d}{E^{\Omega}_{d,\max}} = \frac{A_c}{A^{\Omega}_{c,\max}}. \tag{56}$$

The dependence of the normalized dissipated energy $E_d/E^{\Omega}_{d,\max}$ on the frequency of the externally applied voltage ω can be obtained numerically by averaging over several Langevin trajectories obtained with Eq. (48) with Ω and $\mathcal{E}_1$ fixed and calculating $A_c(\omega)$; see Fig. 5(a). The energy dissipated increases as a function of the frequency until a maximal value $E^{\Omega}_{d,\max}$ is reached at $\omega^{\Omega}_{\max}$. For $\omega > \omega_{\max}$ the

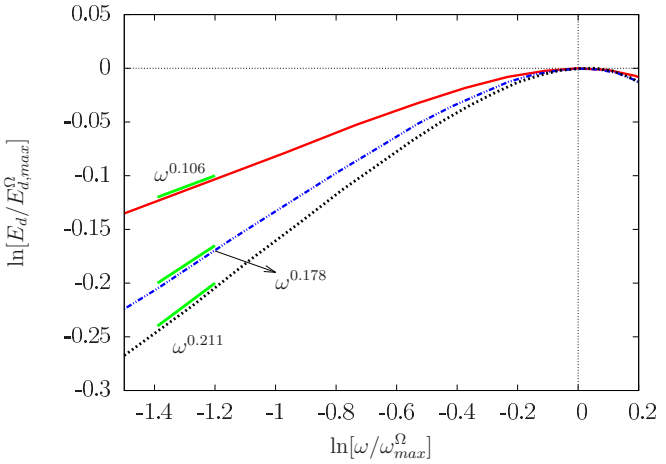

FIG. 6. Normalized dissipated energy dependence for experimental values as a function of frequency. The parameters are $\Omega = 2.75$ (continuous line), $\omega_{\max} = 0.302$, and $A_{\max} = 0.6$; $\Omega = 2.62$ (dashed line), $\omega_{\max} = 0.46$, and $A_{\max} = 0.57$; $\Omega = 2.56$ (dots), $\omega_{\max} = 0.52$, and $A_{\max} = 0.55$. The fixed parameters are $\mathcal{E}_1 = \mathcal{E}_0 = 0.4$, $k_0 = 0.077\ \mathrm{s}^{-1}$, $\kappa = 0.025$, and $\zeta = 0.025$.

tendency of the dissipated energy is to decrease. A similar study (not shown) can be done by fixing ω and $\mathcal{E}_1$ and changing the amplitude of Ω. The result indicates that the energy dissipation depends in a nonlinear way when increasing the nonideality of the system. When Ω increases the separation between the two minima of the Gibbs free energy and the value of the maximum of the energy barrier also increase. This effect implies that both, the area and the shape of the hysteresis, increase as Ω does, as it shown in Fig. 5(b).

For frequencies in the range $0 < \omega < \omega_{\max}$, the energy dissipated follows a power-law-like behavior in terms of the frequency whose mathematical expression can be written in the form

$$\frac{E_d}{E^{\Omega}_{d,\max}} \simeq \left[\frac{\omega}{\omega^{\Omega}_{\max}}\right]^{\gamma}, \tag{57}$$

where we have introduced the normalizing factor $A^{\Omega}_{\max}(\omega^{\Omega}_{\max})$ for each case. This scaling behavior is shown in Fig. 6 for the three cases of Fig. 3(a), that is, for $\Omega = 2.56$ (black), $\Omega = 2.62$ (blue), and $\Omega = 2.75$ (red).

The model allows us to model systems with voltage-sensitive electrodes, that is electrode materials that may be responsive to the external voltage. For instance, during cycling, the material response to a loading voltage could be different from the unloading process because the volume and internal area of the electrodes changes in a different way. These types of effects effects would translate in a asymmetry in the hysteresis loop.

There are two limiting cases of interest that can be illustrated. The first one corresponds to a material that opposes to the load-unload processes. In this case $\Omega(\mathcal{E}_1)$ is maximal at $\mathcal{E}_1 = 0$ and zero at $\mathcal{E}_1 = \mathcal{E}_{1,\max}, \mathcal{E}_{1,\min}$. This can be modeled with a tent function and labeled with $\Omega_{\wedge}(\mathcal{E}_1)$, where the symbol at the subindex schematically indicates the dependence of Ω on the applied voltage. On the contrary, a material that favors the load-unload process would be maximal at $\mathcal{E} = \mathcal{E}_{1,\max}, \mathcal{E}_{1,\min}$

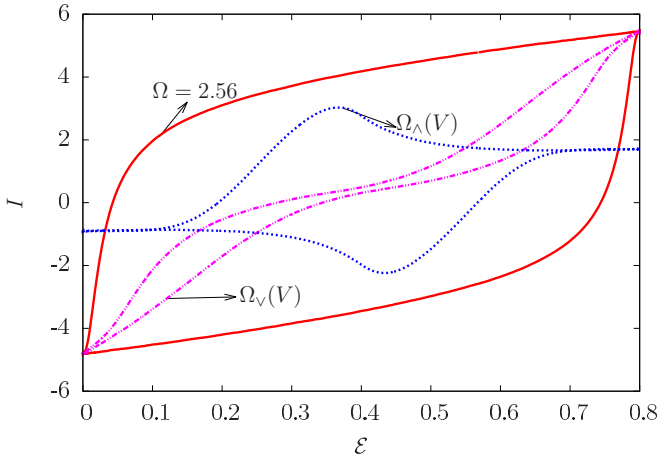

FIG. 7. Hysteresis loops for a nonconstant regular parameter $\Omega_\wedge(V)$ and $\Omega_\vee(V)$ compared to fixed $\Omega = 2.56$; all curve parameters are $\mathcal{E}_1 = 0.4$, $w = 0.2748$, $\zeta = 0.025$, and $\Omega_{\max} = 2.56$.

and zero at $\mathcal{E}_1 = 0$. This can be modeled, in turn, by a linear function labeled with $\Omega_\vee(\mathcal{E}_1)$. Figure 7 shows how the hysteresis cycle becomes affected in these limiting cases. Notice that the area of the cycle, that is, the dissipated energy, decreases in both cases.

VI. CONCLUSIONS

In this work we have formulated a theoretical model that accounts for the main features of the loading-unloading process of a symmetric redox supercapacitor dominated by fast electrochemical reactions at the electrodes.

First we have analyzed the general description of an electrochemical cell in terms of nonequilibrium thermodynamics. We have derived a very general expression for the current-overpotential equation and shown how it can be reduced to the classical current-overpotential and Butler-Volmer equations by successive approximations.

Once proved that our general analysis is consistent with classical works, we have elaborated a basic model of the electrochemical reaction taking place at the electrodes of an MnO_2-based supercapacitor. Using this information and the rules of nonequilibrium thermodynamics, we were able to deduce the form of the nonequilibrium electrochemical affinity, Eq. (46). As a consequence of this, we were able to deduce a very general forms for the load-voltage and current-voltage equations [Eqs. (48) and (50)] that describe galvanostatic and voltametric experiments, respectively.

In the most elemental case, the electrochemical affinity follows a regular mixture law in which the regular parameter is a measure of the departure of the system with respect to ideality. We have show that this law follows from assuming a linear Vegard's law connecting the actual composition of the electrodes with their pure states.

Solving the load-voltage equation (48) we were able to describe the galvanostatic diagram, and, using this information into Eq. (50), we obtained a typical hysteresis cycle of the voltametric diagram. We have fitted experimental data for three different sweep rates. The fits are acceptable good taking into account that we have assumed oversimplified voltage protocols.

Notwithstanding, we consider that the main result of our work is to show that, for a wide range of frequencies previous to reach a maximum value, the energy dissipated per cycle depends on the external voltage frequency ω as a power law. It is also shown that this behavior is sensitive to the value of the nonideal parameter Ω. The existence of a maximum for the energy dissipated as a function of the frequency implies a more intense entropy production per unit time by the electrochemical reactions, and therefore the largest number of electrons exchanged by the system. This suggests the that the corresponding optimal operation frequency should be similar in value to $\omega_{\max}$.

Although the basic model we have formulated here can be generalized in different ways in order to account for more complex systems in which ion insertion, diffusion, and surface and volumetric effects can be important, we believe that our model is a ready-to-use tool in the modeling and performance evaluation of electrochemical systems controlled by fast very electrochemical reactions at the electrodes.

ACKNOWLEDGMENTS

N.P.-A. acknowledges CONACyT for financial support under Ph.D. scholarship CVU 210757. We acknowledge UNAM-DGAPA for financial support under Grant No. PAPIIT-IN116617.

[1] A. S. Aricó, P. Bruce, B. Scrosati, J. M Tarascon, and W. Van Schalkwijk, Nat. Mater. **4**, 366 (2005).
[2] B. E Conway, *Electrochemical Supercapacitors: Scientific Fundamentals and Technological Applications* (Kluwer Academic/Plenum Publishers, New York, 1999).
[3] V. Augustyn, P. Simon, and B. Dunn, Energy Environ. Sci. **7**, 1597 (2014).
[4] A. Burke, J. Power Sources **91**, 37 (2000).
[5] R. Kötz and M. Carlen, Electrochim. Acta **45**, 2483 (2000).
[6] G. Wang, L. Zhang, and J. Zhang, Chem. Soc. Rev. **41**, 797 (2012).
[7] P. Simon and Y. Gogotsi, Nat. Mater. **7**, 845 (2008).
[8] B. E. Conway, V. Birss, and J. Wojtowicz, J. Power Sources **66**, 1 (1997).
[9] H. Lee and J. B. Goodenough, J. Solid State Chem. **144**, 220 (1999).
[10] W. Deng, X. Ji, Q. Chen, and C. E. Banks, RSC Adv. **1**, 1171 (2011).
[11] S. Sarangapani, B. V. Tilak, and C. P. Chen, J. Electrochem. Soc. **143**, 3791 (1996).
[12] I. Santamaría-Holek, N. J. López-Alamilla, M. Hidalgo-Soria, and A. Pérez-Madrid, Phys. Rev. E **91**, 062714 (2015).
[13] M. Hidalgo-Soria, A. Pérez-Madrid, and I. Santamaría-Holek, Phys. Rev. E **92**, 062708 (2015).

[14] T. R. Ferguson and M. Z. Bazant, Electrochim. Acta **146**, 89 (2014).
[15] W. Dreyer, J. Jamnik, C. Guhlke, R. Huth, J. Moškon, and M. Gaberšček, Nat. Mater. **9**, 448 (2010).
[16] R. D. Engelken and T. P. Van Doren, J. Electrochem. Soc. **132**, 2904 (1985).
[17] A. S. Ioselevich and A. A. Kornyshev, Fuel Cells **1**, 40 (2001).
[18] M. Doyle, T. F. Fuller, and J. Newman, J. Electrochem. Soc. **140**, 1526 (1993).
[19] A. Latz and J. Zausch, Electrochim. Acta **110**, 358 (2013).
[20] M. Z. Bazant, Acc. Chem. Res. **46**, 1144 (2013).
[21] R. Parsons, Trans. Faraday Soc. **54**, 1053 (1958).
[22] V. G. Levich, *Physicochemical Hydrodynamics* (Prentice Hall, Englewood Cliffs, NJ, 1962).
[23] M. Van Soestbergen, Russ. J. Electrochem. **48**, 570 (2012).
[24] W. Dreyer, C. Guhlke, and R. Müller, Phys. Chem. Chem. Phys. **18**, 24966 (2016).
[25] M. Rao, H. R. Krishnamurthy, and R. Pandit, Phys. Rev. B **42**, 856 (1990).
[26] P. Jung, G. Gray, R. Roy, and P. Mandel, Phys. Rev. Lett. **65**, 1873 (1990).
[27] W. S. Lo and R. A Pelcovits, Phys. Rev. A **42**, 7471 (1990).
[28] G. P. Zheng and J. X. Zhang, Phys. Rev. E **58**, R1187(R) (1998).
[29] M. Rao, Phys. Rev. Lett. **68**, 1436 (1992).
[30] N. Berglund and B. Gentz, Nonlinearity **15**, 605 (2002).
[31] A. J. Bard and L. R. Faulkner, *Fundamentals and Applications: Electrochemical Methods* (Wiley, New York, 2001).
[32] S. Glasstone, K. J. Laidler, and H. Eyring, *The Theory of Rate Processes: The Kinetics of Chemical Reactions, Viscosity, Diffusion and Electrochemical Phenomena* (McGraw-Hill, New York, 1941).
[33] A. J. Bard, G. Inzelt, and F. Scholz, eds., *Electrochemical Dictionary* (Springer Science & Business Media, Heidelberg, 2008).
[34] S. N. Lvov, *Introduction to Electrochemical Science and Engineering* (CRC Press, Boca Raton, FL, 2015).
[35] J. M. Rubi and S. Kjelstrup, J. Phys. Chem. B **107**, 13471 (2003).
[36] S. Kjelstrup, and D. Bedeaux, *Non-equilibrium Thermodynamics of Heterogeneous Systems* (World Scientific, Singapore, 2008).
[37] D. Bedeaux, S. Kjerlstrup, and J. V. Sengers, *Experimental Thermodynamics, Volume X: Non-equilibrium Thermodynamics with Applications* (Royal Society of Chemistry, Croydon, 2015).
[38] I. Santamaría-Holek, Z. J. Grzywna, and J. M. Rubi, R. Eur. Phys. J. Spec. Top. **222**, 129 (2013).
[39] A. Ledesma-Durán, S. I. Hernández-Hernández, and I. Santamaría-Holek, J. Phys. Chem. C **120**, 7810 (2016).
[40] D. Kondepudi and I. Prigogine, *Modern Thermodynamics: From Heat Engines to Dissipative Structures* (John Wiley & Sons, Chichester, 2014).
[41] Y. Demirel, *Nonequilibrium Thermodynamics: Transport and Rate Processes in Physical, Chemical and Biological Systems* (Elsevier, Amsterdam, 2014).
[42] I. Santamaría-Holek and A. Pérez-Madrid, Phys. Rev. E **89**, 012144 (2014).
[43] R. A. Marcus, J. Chem. Phys. **24**, 966 (1956).
[44] V. Compañ, M. L. Lopez, T. S. Soerensen, and J. Garrido, J. Phys. Chem. **98**, 9013 (1994).
[45] J. Garrido, V. Compañ, V. M. Aguilella, and S. Mafé, Electrochim. Acta **35**, 705 (1990).
[46] M. Toupin, T. Brousse, and D. Bélanger, Chem. Mater. **16**, 3184 (2004).
[47] I. F. Levine, *Physical Chemistry* (McGraw-Hill, Boston, 2002).
[48] A. Frumkin, Z. Phys. Chem. **164A**, 121 (1933).
[49] L. Vegard, Z. Phys. **5**, 17 (1921).
[50] H. W. King, J. Mater. Sci. **1**, 79 (1966).
[51] A. R. Denton and N. W. Ashcroft, Phys. Rev. A **43**, 3161 (1991).
[52] C. Graham and D. Talay, *Stochastic Simulation and Monte Carlo Methods: Mathematical Foundations of Stochastic Simulation* (Springer-Verlag, Heidelberg, 2013).
[53] S. Ardizzone, G. Fregonara, and S. Trasatti, Electrochim. Acta **35**, 263 (1990).
[54] J. Zhi, O. Reiser, and F. Huang, ACS Appl. Mater. Interfaces **8**, 8452 (2016).